

## Initiation of Detonation of a Porous High Explosive by a High-Enthalpy Gas Flow

A. P. Ershov<sup>a</sup>, A. O. Kashkarov<sup>a</sup>,  
L. A. Luk'yanchikov<sup>a</sup>, and E. R. Prueel<sup>a</sup>

UDC 662.215.1

Translated from *Fizika Goreniya i Vzryva*, Vol. 49, No. 1, pp. 91–105, January–February, 2013.  
Original article submitted November 24, 2011.

**Abstract:** Loose packed PETN initiation by a hot gas flow generated by an explosion of an active charge separated by an air gap is studied. Experimental data obtained by means of synchrotron radiography are compared with simulations employing a two-phase two-velocity two-temperature model. Reasonable agreement is reached by taking into account two processes accelerating the reaction: particle fragmentation during powder compaction and combustion intensification due to instability of the evaporating surface layer excited by a high-velocity gas flow around the particles.

**Keywords:** initiation, porous high explosive, deflagration-to-detonation transition.

**DOI:** 10.1134/S0010508213010097

### INTRODUCTION

Initiation of detonation of high explosives (HEs) is the classical problem of explosion physics. Initiation by comparatively weak action is of particular interest. In such cases, the gas-dynamic parameters of the process increase by several orders of magnitude, and the leading mechanisms can change in the course of detonation development. Sensitivity to weak actions determines the safety of operating with HEs. Consequences of unauthorized development of detonation can be extremely severe. This fact justifies the efforts aimed at studying the nature of such processes. Low-density (loose packed) HEs are known to be rather sensitive. Therefore, low-density HEs are most important from the viewpoint of safety.

The majority of studies of HE detonation initiation can be classified into two groups: shock-wave initiation (SWI) and deflagration-to-detonation transition (DDT). Shock-wave initiation is a comparatively fast process: detonation develops within microseconds [1–3]. In most cases, the SWI process was studied for dense (low-porosity) HEs because of their greater efficiency. In addition, the traditional experimental techniques are more suitable for working with dense materials, whereas experimental records obtained for low-density

substances display natural fluctuations because of inevitable inhomogeneities at the HE grain scale.

The DDT process initiated by a much weaker action (usually, by ignition at atmospheric pressure) is much slower. Detonation development takes milliseconds or, at least, tens of microseconds [4–6]. The desire to ensure reproducibility of the experiment and simplify its interpretation imposed rather severe restrictions. The classical DDT requires the HE to be confined within a strong casing (usually, a thick-walled steel tube) restrict side expansion of combustion products to facilitate one-dimensional process development. Such a configuration can belong to natural ones, and DDT conditions determined by this classical approach can be appreciably different from real situations of unauthorized detonation, which can occur, for instance, during HE transportation. In some later works, no igniter was used at all: combustion was initiated by a piston compressing the HE from one of the charge end faces (see [7]). In such experiments, more rigorous one-dimensionality was presumably reached, owing to prevention of the emergence of longitudinal channels through which the flame can propagate. However, this version is yet more remote from the typical conditions of natural DDT.

There are also processes called XDT (X stands for an “unknown factor,” i.e., detonation is induced under conditions that differ from those of SWI and DDT [8]). Such a process can be initiated, for instance, by an im-

<sup>a</sup>Lavrent'ev Institute of Hydrodynamics, Siberian Branch, Russian Academy of Sciences, Novosibirsk, 630090 Russia; ers@hydro.nsc.ru.

pact with a velocity insufficient for standard SWI and may not require strong confinement. In terms of its development time and destructive effect, XDT is an intermediate variant between SWI and DDT. It is believed that XDT develops owing to intense shear deformations destroying the HE.

It should be noted that the boundaries between different detonation modes are rather conventional. In any case, detonation development is impossible without HE ignition and generation of gaseous reaction products. In the SWI case, heated gas regions (hot spots) in solid HEs appear owing to pore collapsing, friction, strains, etc., as the HE is compressed by an impermeable piston, i.e., the gas in combustion spots is generated from the HE itself. In the DDT case, standard initiation is performed by an igniter, which is an external source of the hot gas, though the “piston” variant of DDT and XDT do not involve the use of an external igniter. A greater distinction is seen in the different velocities of the process, with SWI duration confined within the microsecond interval.

Somewhat apart from the phenomena considered above stands detonation initiation by an explosion of a remote active charge. Numerous data on detonation transfer through an air gap are mainly of an empirical character. The transfer mechanisms are still under discussion: the initiation factors are believed to be the shock wave in the receiving charge, heating by active charge detonation products, compression of gas inclusions, etc. Against this background, the classical work [9] should be mentioned, in which powdered HEs were initiated through an air gap quite rapidly. In loose packed RDX, detonation developed in less than 10  $\mu$ s, though the stagnation pressure of the flow was only 65 MPa. Thus, the characteristic time of initiation was close to the SWI case, though the acting pressure was much lower. Belyaev et al. [9] concluded that the initiating agent was a hot gas flow behind the air shock penetrating into the pores and igniting the HE. Actually, an extremely fast case of the deflagration-to-detonation transition occurred. It should be noted that such rapid excitation did not require strong confinement because the charge is effectively confined by inertia at microsecond scales.

Later other methods were found to obtain similar processes, such as an electric discharge or a wire explosion inside a powdered HE, injection of hot combustion products from a separate chamber after the membrane between the chambers was broken, and an impact of a gas detonation wave [10–12]. In these cases, the gas pressure at the boundary with the powdered HE also amounted to merely hundreds of atmospheres, but an important factor was abrupt application of the initiat-

ing action. The nature of rapid detonation development after initiation by a weak source is of obvious interest. Observations allow us to argue that the two-phase character of the process is essential. Actually we have an extremely fast DDT. After intense injection of a hot gas into the HE pores, the detonation transition starts from a stage of comparatively fast convective burning. The slowest stage of layer-by-layer combustion typical for the classical DDT is bypassed.

In this work, initiation of low-density powdered PETN is studied by using a new physical method, namely, charge radiography with the use of a synchrotron radiation (SR) beam. The measurements were performed at the Siberian Center of Synchrotron Radiation (Center at the Budker Institute of Nuclear Physics of the Siberian Branch of the Russian Academy of Sciences), at the Vzryv (“Explosion”) experimental station. Synchrotron diagnostics is practically non-perturbative, allows observations to be performed in the charge interior, and appreciably increases the amount of information extracted from experiments. Naturally, reconstruction of distributions of physical fields (e.g., density fields) requires profound mathematical support. To study the mechanism of the process, we compare the density distributions with the results calculated by a two-phase two-velocity gas-dynamic model. The model takes into account various mechanisms of phase interaction. New data allowed us to perform a detailed comparison of the experimental and simulated density profiles and to estimate the role of the basic initiation factors.

## EXPERIMENT

As in [9], a high-enthalpy gas flow was generated by an explosion of an active charge separated by an air gap from the examined porous HE. A cylindrical PETN charge (16 mm in diameter and 25 mm long) in a thin plastic casing was initiated. The grain size of PETN was approximately 0.3 mm. Injection of hot air from the open end face of the examined charge caused a complicated two-phase flow. The dynamics of this flow was monitored by means of synchrotron radiography. The experimental arrangement is illustrated in Fig. 1.

Synchrotron radiation is a high-intensity beam of bremsstrahlung photons with an energy of 10–30 keV. Actually, the accelerator operates as a high-quality source of soft x-ray radiation. The angular divergence of SR is rather low: the radiation is focused in a narrow cone around a velocity vector with an angle of the order of  $1/\gamma$ , where  $\gamma$  is the relativistic factor. If the electron energy is several gigaelectronvolts, the divergence angle

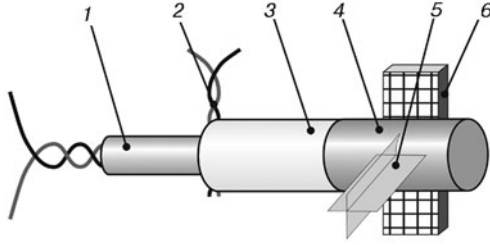


**Fig. 1.** Initiation system and charge position with respect to the SR beam: (1) detonator; (2) contact sensor; (3) air gap; (4) examined HE charge; (5) SR beam; (6) detector.

has the order of  $10^{-3}$  to  $10^{-4}$  rad. Radiation pulses are repeated with a period of orbital rotation of the electron beam (250 ns for the VEPP-3 accelerator), and the pulse duration is about 1 ns. In principle, SR is generated at all segments that have some orbit curvature and, therefore, transverse acceleration. For SR amplification, however, special segments (wigglers) with a magnetic field of alternate signs are organized, in which the trajectory resembles a snake. The SR beam leaving the wiggler had the shape of a band with a cross section of  $20 \times 0.1$  mm. The radiation was detected by a linear gas detector with a spatial resolution of 0.1 mm [13, 14].

SR absorption is determined by the integral of density along the beam and does not depend on chemical processes in the medium. The intensity of the transmitted radiation was measured along the charge axis to determine the general dynamics of process evolution and in several cross sections with a time step of  $0.5 \mu\text{s}$  determined by the accelerator period and available rate of information readout. Figure 1 shows both possible arrangements of the beam plane with respect to the charge; in reality, either longitudinal or transverse transmission was used.

In experiments with transverse measurements, we determined the dynamics of x-ray shadow and the density distributions over the radius in a fixed examined cross section. Density reconstruction was based on the x-ray shadow from one viewing direction, and the distribution of the material was assumed to be cylindrically symmetric.

To reconstruct the density dependence on the radius and time in a fixed cross section, the density dynamics as a function of time at some reference points (four points over the radius) was approximated by a spline function containing five points in time. The following specific features of the flow were taken into account when the positions of the reference points were chosen: the splines with respect to time on the radii inside the charge started on the front of the curved initi-

ation wave; outside the initial charge radius, the splines started at the outer boundary charge material expansion into the atmosphere.

Using the above-described set of parameters (20 values of density at the reference points and two additional parameters: front curvature and spreading angle), we reconstructed the density dynamics only at some reference points along the radius. Reconstruction of density at an arbitrary point of the radius was based on spline interpolation of data.

To reconstruct the dependence of density on the radius and time in an arbitrary cross section, we constructed interpolation splines along the charge axis (generally, five reference points) for all parameters mentioned above. A total of approximately 100 real parameters were used to describe the density distribution. The algorithm of density dynamics reconstruction was based on choosing these parameters under the conditions of minimizing the sum of the squared deviations of the calculated values of x-ray densities from the experimentally measured results. A special computer code implementing the algorithm searching for an extreme point of a nonlinear function of multiple variables on the basis of the simplex method was written for minimization.

In choosing the density parameters, we used transverse x-ray shadows obtained in different charge cross sections in different experiments performed under identical initial conditions. To attach the results to a unified timeline of the process, we used the data of longitudinal x-ray radiography where the front coordinate was measured in one experiment as a function of time. Thus, we determined the two-dimensional dynamics of the process: dependence of the mean density of the material  $\bar{\rho}$  on the radius  $r$ , axial coordinate  $x$ , and time  $t$ . The experimental procedure was described in more detail in [15, 16].

The intensity of the flow acting on the charge under study was regulated by varying the primary active charge. The first impact on the powder is exerted by the hot gas plug behind the air shock. The fate of the process is determined by this action (during the first microseconds). All parameters of the initiating flow were determined from the measured velocity of the air shock. The impact of the air plug is similar to the action of HE combustion products or gaseous detonation products, which were used in [10–12].

Of the main interest is the near-critical initiation mode, for which the gas flow velocity immediately before the contact with the powder was  $u = 2.2$  km/s and the pressure in the incident air shock was  $p \approx 10$  MPa. Thus, the pressure after reflection from a rigid wall was 90 MPa, which is substantially lower than the value needed for shock-wave excitation of PETN detonation.

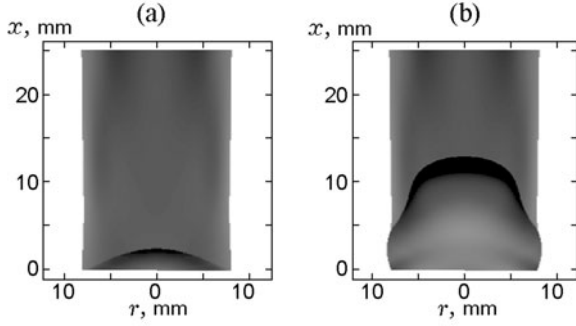


**Fig. 2.** Density distribution in the axial plane of the charge at near-critical initiation: 3 (a) and 8  $\mu\text{s}$  (b) after the beginning of gas flow penetration into the powder.

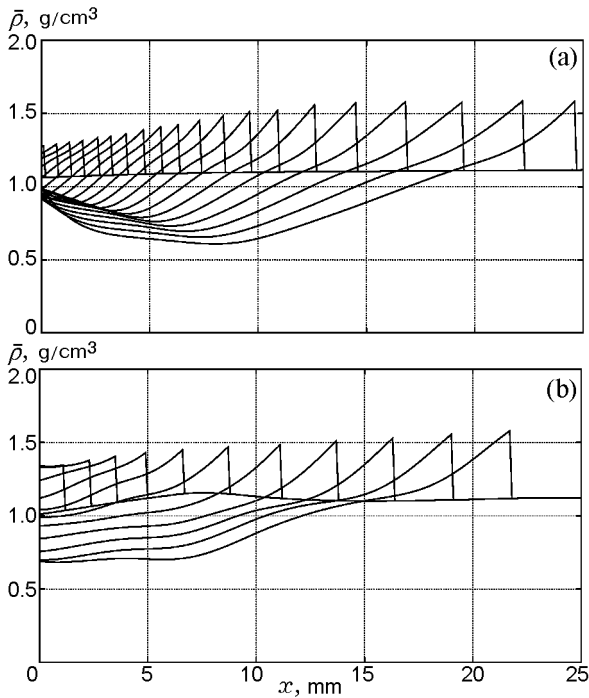


**Fig. 3.** Density distribution along the charge axis: (a) mild initiation mode, time of the process 9.5  $\mu\text{s}$ ; (b) strong initiation mode, time of the process 5.5  $\mu\text{s}$ ; the time step between the profiles is 0.5  $\mu\text{s}$ .

For instance, the minimum SWI pressure of 250 MPa was found in [17] for a more sensitive fine-grain PETN. Examples of two-dimensional density distributions obtained in this regime are shown in Fig. 2.

To compare the experimental data and the simulations by the numerical model described below, a series of density profiles on the charge axis was used. Figure 3 shows two sets of profiles obtained in two series of experiments. Figure 3a illustrates the above-mentioned near-critical or “mild” initiation case. The wave veloc-

ity in the powder is approximately 1 km/s at the beginning, increasing to 5 km/s at the end of the process. Therefore, practically normal detonation regime develops within 10  $\mu\text{s}$ . Figure 3b demonstrates a “strong” regime for which the initial velocity of the gas flow is  $u = 4.5$  km/s and the pressure is  $p = 30$  MPa, which corresponds to the pressure after reflection of about 300 MPa. Naturally, the detonation development in this case is much faster.

A monotonic increase in the peak density on the reconstructed profiles and gradual acceleration of the wave should be noted. Another typical feature, especially for the “mild” regime of initiation, is moderate compression reached within several first microseconds. It means that the powder remains permeable for the gas at the beginning of the process (there is no dense compacted region). For this reason, the leading role in wave propagation at the initial stage of initiation can be preliminary assigned to filtration of hot gases.

## NUMERICAL MODEL

The amount of information that can be extracted from a synchrotron experiment allows a detailed comparison with the numerical model of the process. One can expect that such a comparison would provide better understanding of the initiation mechanism. The model must take into account all important factors, but it should not be overcomplicated. As was noted above, for the “mild” impact of the hot gas on loose packed PETN, the initiation agent is not the shock wave in the powder (for which a one-velocity description of the medium could be used). The gas flow entering the powder is smoothly decelerated, and acceleration of the HE particles is all the more gradual. The shock wave (if any) in the powder is formed at a comparatively late stage. A critical factor for our problem is interaction of the phases: filtered gas and solid grains. Based on these considerations, we decided to use a two-phase two-velocity two-temperature model. As is seen from Fig. 2, there is only minor side expansion of the charge, even at late stages of the process. Though the compression wave curvature is visible, its role does not seem to be essential near the charge axis; thus, a one-dimensional approximation is acceptable.

The computational domain is divided into two parts. The subdomain  $0 < x < 25$  mm is occupied by the PETN charge with a porosity  $\varphi_0 = 0.42$ ; the pores are filled by air under standard conditions. The subdomain  $0 > x > -50$  mm includes the air gap and the active charge. These sizes are the same as those used in experiments.

The governing equations have the following form:

$$\begin{aligned}
& \frac{\partial \rho \varphi}{\partial t} + \frac{\partial \rho \varphi u}{\partial x} = J, \\
& \frac{\partial \rho \varphi u}{\partial t} + \frac{\partial \rho \varphi u^2}{\partial x} + \varphi \frac{\partial p}{\partial x} = Jv - f, \\
& \frac{\partial \rho \varphi E_g}{\partial t} + \frac{\partial \rho \varphi u E_g}{\partial x} + p \frac{\partial (\varphi u + \alpha v)}{\partial x} \\
& = J \left[ Q + \frac{(u - v)^2}{2} + E_s \right] + f(u - v) - q, \\
& \rho_s \left( \frac{\partial \alpha}{\partial t} + \frac{\partial \alpha v}{\partial x} \right) = -J, \\
& \frac{\partial v}{\partial t} + \frac{1}{2} \frac{\partial v^2}{\partial x} + \frac{1}{\rho_s} \frac{\partial p}{\partial x} + \frac{1}{\rho_s \alpha} \frac{\partial p_s}{\partial x} = \frac{f}{\rho_s \alpha}, \\
& \frac{\partial E_s}{\partial t} + v \frac{\partial E_s}{\partial x} + \frac{p_s}{\rho_s \alpha} \frac{\partial v}{\partial x} = \frac{q}{\rho_s \alpha}, \\
& p_s = p_s(\varphi, \varphi_{\min}), \quad E_s = C(T_s - T_0) + E_p, \\
& p = p(\rho, E_g), \quad T = T(\rho, E_g).
\end{aligned} \tag{1}$$

Here  $\rho$  is the gas density,  $\rho_s$  is the density of explosive grains (assumed to be constant),  $\alpha$  is the volume fraction of the solid phase,  $\varphi$  is the porosity,  $\alpha + \varphi = 1$ ,  $u$  is the gas velocity,  $v$  is the solid phase velocity,  $E_g$  and  $E_s$  are the internal energies of the gas and solid phase,  $p$  is the gas pressure,  $p_s$  is the pressure of compression of the solid bed,  $T$  and  $T_s$  are the temperatures of the gas and solid phase,  $C$  is the heat capacity of the solid,  $f$  is the force of friction between the phases,  $q$  is the heat exchange term,  $J$  is the mass influx from the solid to the gas phase, and  $Q$  is the thermal effect of the reaction. It is assumed that the gas inflow is in the form of combustion products.

System (1) has a generally standard form, except for the equation of motion of the solid, in which the basic variable the solid “velocity.” Usually, the momentum density  $\rho_s \alpha v$  (see, e.g., [18]) is used, and the velocity  $v$  is obtained through division by  $\alpha$ , which vanishes in some flow regions in our problem. In the right side of the transformed equation, division of  $f/(\rho_s \alpha)$  by zero is avoided as the factor  $\alpha$  enters the resistance (drag) force (see below). The “solid” pressure  $p_s$  appears only at values  $\alpha > 1 - \varphi_0$ , which are strictly positive. To suppress formal instability of the problem, we used the smoothing scheme developed in [18].

Though the main (differential) parts of the two-phase flow equations follow quite definitely from conservation laws, there is certain arbitrariness in choosing the form of the closing relations, especially those that

describe phase interaction. Actually, these relations determine the “individual features” of the model. Experimental data and/or reasonable theoretical asymptotic solutions are now available for some interactions.

The equation of state of the gas phase  $p = p(\rho, E_g)$  is taken from [19]. This equation is applicable in the entire range of pressures from the initial (atmospheric) to detonation pressure. No distinction was made between air (in charge pores and in the air gap) and combustion/detonation products, because at low pressures the equation [19] describes an ideal gas with the ratio of specific heats equal to 1.375, which is a good approximation for air. At high pressures, the role of air becomes insignificant.

Irreversibility of powder deformation was taken into account in the description of stresses in the solid phase. The pressure in the solid bed during the compression phase is

$$p_s = \rho_s c_{0s}^2 \left[ (1 - \beta)(\varphi_0 - \varphi) + \beta \varphi_0 \left( \frac{\varphi_0}{\varphi} - 1 \right) \right]. \tag{2}$$

Here  $c_{0s}$  is the velocity of sound in the solid bed in the initial state ( $\varphi = \varphi_0 = 0.42$ ) and  $\beta$  is the fitting coefficient. The parameters  $\beta = 0.25$  and  $c_{0s} = 0.22$  km/s were chosen to fit the data [20] (see Fig. 4). For comparison, Fig. 4 also shows the function used in [21]. At moderate compression, it is similar to dependence (2). When all pores are closed, however, the dependence [21] yields a finite (and rather low) pressure value. Dependence (2) implies incompressibility of the void-free solid (the pressure tends to infinity as  $\varphi \rightarrow 0$ ), which is in better agreement with the experiment. In the most interesting regimes described below, the main events occur at pressures within hundreds of megapascals, and complete closure of the pores is not reached; therefore, the compressibility of PETN crystals plays a minor role.

Noticeable compaction of the powder at comparatively low pressures is caused by fragmentation of HE grains with filling of the pores by these fragments, i.e., the deformation is irreversible. To reflect this effect, we introduced a special variable into Eq. (1):  $\varphi_{\min}$ , which is the minimum porosity reached at a given place (Lagrangian point) previously. Thus, the material “memorizes” the state of its maximum compression. Equation (2) is satisfied at the loading stage, i.e., at  $\varphi < \varphi_{\min} \leq \varphi_0$ . For the unloading stage, the stress is assumed to decrease linearly, with the derivative reached at  $\varphi_{\min}$  (see Fig. 4). Naturally, only non-negative values of pressure are allowed. If unloading stage is succeeded by new compression, the pressure is first recovered along the current unloading curve and then, after  $\varphi = \varphi_{\min}$  is reached, again follows the dependence given by Eq. (2).

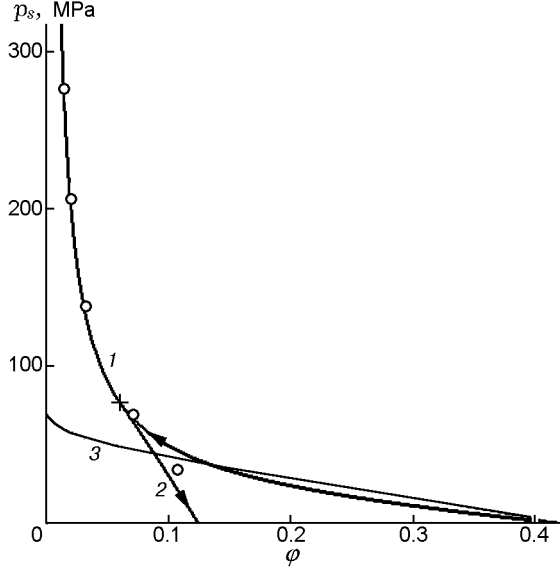


**Fig. 4.** Pressure of the solid phase versus porosity: the open points are the experimental data [20]; curve 1 is dependence (2) at the stage of compression; curve 2 shows the decrease in pressure at the stage of unloading; the beginning of the unloading stage is indicated by the cross; curve 3 is the dependence used in [21].

Given the known stresses, the elastic part  $E_p$  of the solid phase energy, i.e., the work to be released during unloading, can be easily found. The expression is rather cumbersome and is not given here. Note that the remaining part of the powder compression work is spent on solid phase heating.

For the friction force between the phases, we used the classical Ergun's correlation [22] with a correction factor of 0.5, which takes into account the later data [23],

$$f = 0.5S \frac{1-\varphi}{\varphi} \frac{\rho|u-v|(u-v)}{d} \left( 1.75 + \frac{150}{\text{Re}_d \varphi} \right), \quad (3)$$

where  $d$  is the explosive grain size and  $\text{Re}_d$  is the Reynolds number determined from the relative velocity of the phases and the particle diameter. At flow velocities of hundreds meters per second, the Reynolds number is of the order of hundreds of thousands; therefore, the resistance is essentially a quadratic function of velocity.

The heat exchange between the gas and the particles was expressed in accordance with Denton's formula [24]

$$q = \text{Nu}AS \frac{\lambda(T - T_s)}{d}, \quad (4)$$

$$\text{Nu} = 2 + 0.6 \left( \frac{\rho|u-v|d\varphi}{\eta} \right)^{0.7},$$

where  $\lambda$  is the thermal conductivity of the gas,  $\text{Nu}$  is the Nusselt number,  $\eta$  is the dynamic viscosity of the gas, and  $A$  is the specific surface (per unit volume) of the powder. In the initial state ( $\varphi = \varphi_0$ ), we have  $A = 6(1 - \varphi_0)/d$  for spherical grains. The coefficient  $S$  in Eqs. (3) and (4) reflects a possible increase in the specific surface owing to fragmentation of particles. The dependences used for  $S$  are given below. The kinetic coefficients  $\lambda$  and  $\eta$  were determined for the composition of the products  $5\text{H}_2\text{O} + 2\text{N}_2 + 3\text{CO} + 2\text{CO}_2$  from the data reported in [25] under the assumption of validity of asymptotic dependences for an ideal gas. Radiative heat transfer was also taken into account by using standard formulas for blackbody radiation.

## IGNITION AND COMBUSTION LAW

Mass transfer between the phases is the most complicated problem. It is the gas inflow rate (reaction intensity) that determines the fate of the process. An analysis showed that the commonly accepted laws for the mass transfer  $J$  are not reliable in the domain of parameters considered in our study and have to be modified to fit the experiment. The approaches used for this purpose are described in this section.

In the model used here, the combustion begins when the particle ignition condition is satisfied. In practice, such a condition may be, for example, a certain surface temperature of the grains [26]. For this purpose, it is necessary to introduce the temperature distribution in the particles, which is determined in the course of calculations. An ignition condition consistent with the reaction kinetics (see, e.g., [27, 28]) seems to be more reasonable. These approaches are close to each other in the cases of a strong dependence of the reaction rate on temperature.

It turned out that the approach developed in [27, 28] yields unrealistically short ignition times, given extremely high heat fluxes typical for our problem. Indeed, at a pressure of 50 MPa, filtration rate  $u - v \simeq 1$  km/s, and gas temperature of 4000 K, the heat flux  $G$  is approximately  $2.5 \cdot 10^{-3}$  J/(mm<sup>2</sup> · μs). For a constant flow, ignition in accordance with [27] occurs at an instant when the rate of heat release in the heated layer owing to the chemical reaction becomes equal to the heat flux, which yields the formulas

$$\exp \frac{E_a}{RT_b} = \frac{\lambda_s \rho_s Q_d K_0}{E_a} \frac{RT_b^2}{G^2},$$

$$t_k = \frac{\pi \rho_s C \lambda_s (T_b - T_0)^2}{4 G^2},$$

where  $T_b$  is the surface temperature corresponding to the instant of ignition,  $T_0$  is the initial temperature,

$\lambda_s$  is the thermal conductivity of the HE, and  $t_k$  is the “kinetic” ignition time. For the commonly used kinetics of PETN decomposition (activation energy  $E_a = 196.6$  kJ/mol, pre-exponent  $K_0 = 6.3 \cdot 10^{19}$  1/s, and decomposition heat  $Q_d = 1.256$  kJ/g [29]), one can easily find the ignition temperature and time:  $T_b \approx 910$  K and  $t_k \approx 30$  ns. The criterion proposed in [28] (ignition corresponds to the point of inflection in the dependence of the surface temperature on time) yields similar values:  $T_b \approx 830$  K and  $t_k \approx 20$  ns.

Certainly, the kinetic parameters were determined in the region of significantly lower temperatures (and, correspondingly, greater times). Nevertheless, the predicted ignition times  $t_k$  can be considered as an approximate estimate. They should be compared with the characteristic mesoscopic time of the problem, which can be naturally defined as the time of the flow around the particle  $d/(u-v) \simeq 300$  ns. There is no point in considering shorter times of the processes in a model operating with average characteristics of the phases.

Thus, within the framework of the continuum approach, the thermal theory of ignition predicts almost instantaneous ignition of particles. The following problem arises here. In a standard model, when the ignition condition is satisfied, the particle is considered as a reacting particle. After that, the heat transfer is ignored and the mass transfer  $J$  is determined by the normal burning rate  $u_n$ , for which data obtained under steady conditions are available in the literature. If the ignition time is of the order of 25 ns, however, the thickness of the heated layer on the particle surface in a material with the thermal diffusivity  $\chi \simeq 10^{-3}$  cm<sup>2</sup>/s does not exceed  $5 \cdot 10^{-2}$   $\mu$ m. Such a thin layer is not sustainable, and the heat stored in this layer will be scattered after heating termination, resulting in HE quenching. In practice, at a pressure of 50 MPa corresponding to the steady normal burning rate  $u_n \approx 5$  cm/s, the heated layer should have the thickness  $\chi/u_n \simeq 2$   $\mu$ m; therefore, a much longer time of heating is required. Thus, the classical theory of ignition underestimates the ignition time (needed for development of stable combustion) in our case.

Based on these considerations, Andreev et al. [30] recommended a “steady” criterion: heating is continued until a heated layer corresponding to the normal burning rate  $u_n$  is formed. In this case, the ignition time is estimated as  $t_s \sim \chi/(\pi u_n^2)$ ; in our problem, with the above-mentioned conditions, the ignition time is about 10  $\mu$ s, i.e., it is too long (exceeds the time of detonation development). Moreover, the delay of ignition at the same heat flux should formally lead to an increase in the surface temperature approximately by a factor of  $\sqrt{t_s/t_k}$ , i.e., at least up to  $10^4$  K. Such high tem-

peratures of the condensed phase are obviously outside the reasonable range. Therefore, the “steady” variant should be considered as an estimate from above.

Thus, the considered extreme variants of ignition criteria do not yield physically reasonable results; they rather form brackets containing the real instant of ignition. This could be expected because the classical conditions were obtained for much slower processes. Naturally, they are in bad agreement with our problem. The ignition process can be qualitatively described as follows. The heat flux is high because of the high velocity of the gas flow around the particles. If the flow around the particle surface is sufficiently intense, the gas rapidly mixes with the incoming flow, and heating is not completely terminated after the ignition. Combustion begins earlier than a stable burning layer is formed, but it can proceed for a certain time in the form of consecutive short flashes. If the pressure in the pores increases during this stage to a sufficient level (up to hundreds of megapascals, i.e., severalfold), the normal burning rate  $u_n(p)$  also increases, the thickness of the quasi-steady layer and the time necessary for its heating decrease, and stable combustion by the classical mechanism becomes possible.

A consistent theory of the above-described processes is rather complicated and has not yet been brought to a level that allows its application in a gas-dynamic model. In this work, therefore, we use a rather rough approximation in which ignition, as in [18], occurs when a certain average temperature of the solid phase is reached, i.e., when the particle temperature increases by a given value  $\Delta T_s$ . This value was varied to obtain the best agreement between the simulations and experiments. The limits for  $\Delta T_s$  can be estimated by equating the amount of heat stored in the stable heated layer and the averaged increment of the thermal energy of the particles. If ignition occurs in the model within 1  $\mu$ s at a surface temperature of the order of 1000 K, then  $\Delta T_s$  lies in the interval from several degrees (for the initial grain size) to several tens (after sufficient fragmentation of the particles, with the mean particle size decreased by an order of magnitude).

After ignition, the burning rate is determined by the current pressure of the gas, as it is usually done, and the mass transfer is described by the formula

$$J = ASu_n(p). \quad (5)$$

For PETN, in accordance with [31], in the most important range of pressures up to 400 MPa, the normal burning rate  $u_n$  is proportional to pressure and amounts to 11 cm/s at  $p = 100$  MPa.

Note that the standard kinetics of particle burning from the surface is too slow. Fast development of the process requires higher reaction rates approximately by

an order of magnitude. In our formulation, such enhanced rates are ensured by means of interaction intensification. First, we take into account the increase in the specific surface of phase interaction due to fragmentation of grains under compression, which is reflected by introducing the coefficient  $S$  depending on the minimum porosity  $\varphi_{\min}$  to Eqs. (3)–(5). In our calculations, we used the dependence approximating the data [4]:

$$S = 1 + 4 \left( \frac{1}{\varphi_{\min}} - \frac{1}{\varphi_0} \right). \quad (6)$$

The specific surface increases tenfold if the porosity is  $\varphi_{\min} \simeq 0.2$ .

The second mechanism of interaction intensification taken into account is the process considered in [32]. The action of a high-velocity flow on the HE grains results in intense heat transfer leading to surface evaporation. The evaporating layer is subjected to shear instability whose development favors rapid stalling of the layer and its burnout. Such a model yields the following expression for the burning rate:

$$u_n = \frac{k}{\rho_s} \left( \frac{\lambda}{C_g d} \right)^{1/3} (\rho|u - v|)^{2/3}. \quad (7)$$

Here  $C_g$  is the specific heat of the gas and  $k$  is a coefficient of the order of unity. At the flow velocity  $u - v = 1$  km/s and gas density  $\rho = 0.1$  g/cm<sup>3</sup>, the surface regression rate is approximately 1 m/s. Thus, at parameters typical for our problem, the reaction is accelerated approximately by an order of magnitude. In contrast to the fragmentation effect, such acceleration is also possible for the initial grain size. Below, such a situation is referred to as the ablative combustion mode.

## SIMULATION RESULTS

As was noted above, a series of consecutive density profiles was chosen for comparisons with one-dimensional simulations. In the calculations, the initiating action was determined by the active charge size chosen to ensure required parameters of the initiating air flow. The active charge detonation was assumed to be instantaneous, and the calculation started from expansion of the detonation products into the air gap. The air plug pushed by the detonation products reached the powder boundary after some time. Hot air was filtered to the pore space, beginning the initiation process. A reflected compression wave propagated upstream in air from the boundary. The porous medium created a significant resistance to the flow, so that the reflected wave parameters were not much different from those in the case of reflection from a rigid wall.

The modeling revealed a qualitative difference in the character of the action on the powder in the two initiating regimes mentioned above. In the strong regime, the active charge had a greater size. The products of its detonation retained a higher density during their expansion. The wave reflected from the powder boundary reached the contact discontinuity between the air plug and the “piston” (active charge detonation products) and was reflected again as a strong shock wave. Its arrival on the powder boundary generated the second pressure jump (approximately in 2  $\mu$ s) to a level exceeding 1 GPa. At such powerful actions, a shock wave is rapidly formed in the powder, and detonation evolution by the SWI mechanism should be expected (for which a pressure of only 250 MPa is sufficient [17]). One can hardly expect a two-phase model based on surface combustion kinetics to be adequate in this situation.

Therefore, the main attention was paid to simulation of the mild initiation variant where the second wave was weaker because of the lower contrast in densities on the contact discontinuity and reached the powder boundary much later. The pressure in the air plug near the boundary decreased after the arrival of the first wave because of air filtration to the powder and then again increased in the second wave approximately to the level determined by the first wave. Thus, the external action was always limited by a level below 100 MPa, which was insufficient for SWI.

It was natural to start the modeling from the traditional variant, which does not include reaction intensification. Figure 5 shows the calculated evolution of the process in the mild initiation mode. The contact discontinuity does not reach the powder boundary within the entire calculation time, i.e., the HE is affected indeed by the hot air flow. The initial pressure on the charge boundary is approximately 60 MPa, and the maximum pressure decreases to 37 MPa in 2.5  $\mu$ s. By the time instant  $t = 7$   $\mu$ s, the wave reflected from the contact boundary almost catches up with the front of the first wave in the powder. The pressure slightly increases owing to superposition of the waves at  $t = 10$   $\mu$ s. Leaving aside these fluctuations, the maximum pressure of the gas decreases with time. Initially, the ignition point was ahead of the peak of the maximum compression of the powder owing to intense heat transfer during several first microseconds. Later, the flow is decelerated, the heat transfer becomes less intense, and the ignition point falls behind the maximum compression point. The late initiation of the reaction and its insufficient intensity lead to wave decay. The volume fraction of the solid phase  $\alpha$  and the solid pressure  $p_s$  gradually increase. A dense, not permeable for the gas, plug is formed, which moves rather slowly (the mean velocity

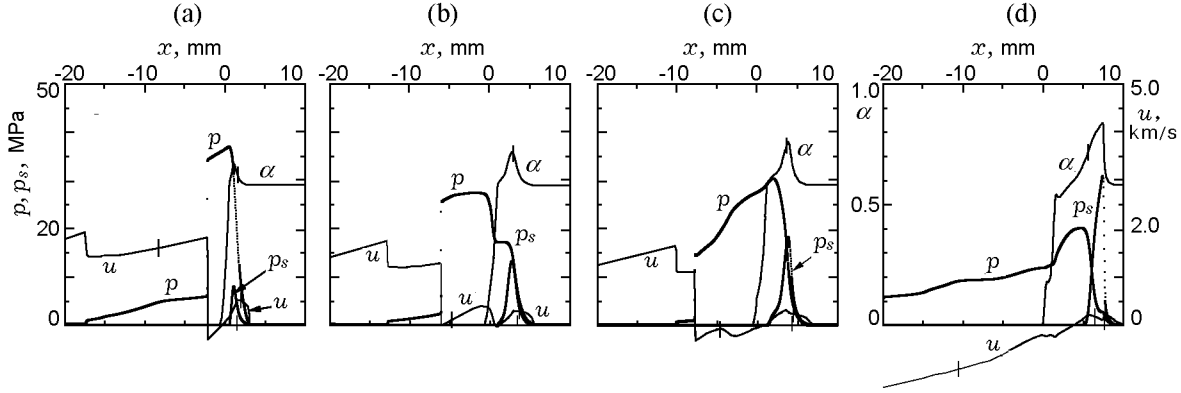


**Fig. 5.** Calculated profiles of flow parameters for the combustion law (5) at  $\Delta T_s = 10$  K: the time after the arrival of the flow on the powder boundary is 2.5 (a), 7 (b), 10 (c), and 20  $\mu$ s (d); the vertical bars on the profiles of  $\alpha$  indicate the place where ignition occurs; the bars on the profiles of  $u$  show the position of the contact discontinuity.

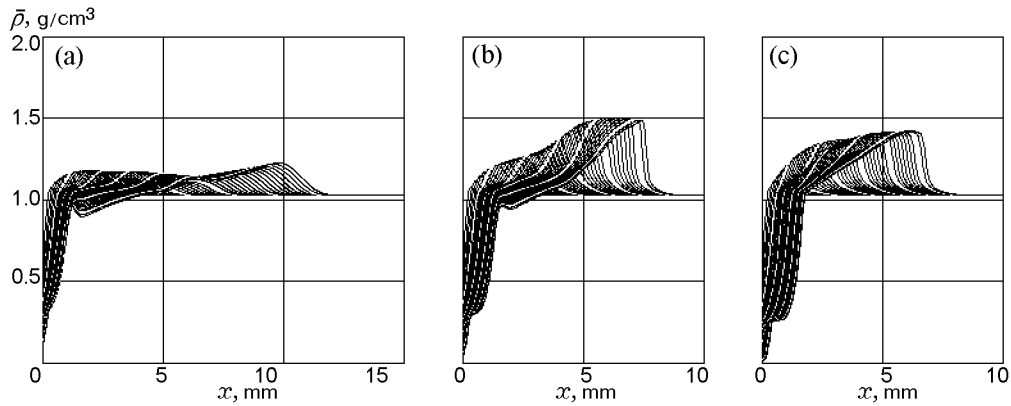


**Fig. 6.** Calculated profiles of density for the combustion law (5): the time step between the profiles is 0.5  $\mu$ s;  $\Delta T_s = 2$  (a), 10 (b), and 40 K (c); the calculation time is 20  $\mu$ s.

of the compression wave in the interval  $0 < t < 20$   $\mu$ s is approximately 400 m/s). At greater times, the plug becomes thicker, the stress and density in the plug decrease, and the velocity of the compression front also decreases. In a real non-one-dimensional situation, such a slow dynamics of the process would lead to failure because of the side expansion.

The inefficiency of the standard kinetics is even more clearly demonstrated by a comparison of the calculated profiles of the mean density  $\bar{\rho} = \rho_s \alpha + \rho \varphi$  shown in Fig. 6 with the experimental data (see Fig. 4a). The simulation predicts a much denser set of the profiles, which corresponds to an extremely slow motion of the wave. Though the calculation time for all variants shown in Fig. 6 was 20  $\mu$ s (twice greater than the experimental time), the wave did not cover even one half of the charge.

To elucidate the role of the ignition condition, we varied the critical temperature  $\Delta T_s$  from 2 to 40 K. At

the low ignition temperature (Fig. 6a), the mean velocity of wave propagation slightly increased during the first 20  $\mu$ s (up to 550 m/s, which is approximately one half of the experimental initial velocity). In this case, however, the amplitudes of the density profiles drastically decreased (down to 1.2 g/cm<sup>3</sup>). At greater values of  $\Delta T_s$  (Fig. 6c), the velocity decreased to 350 m/s, which was in even worse agreement with the experiment. Thus, a comparison with the experiment reveals the absence of any agreement for calculations that ignore reaction intensification at the initial stage of the process. The standard kinetics (5) is too slow to ensure the detonation evolution observed in the experiments.

The growth of the specific surface due to fragmentation of the powder particles intensifies all forms of phase interaction; therefore, the necessity of taking into account the fragmentation effect seems to be natural. The calculations [33] demonstrated that the process can be enhanced by fragmentation. The experimental infor-

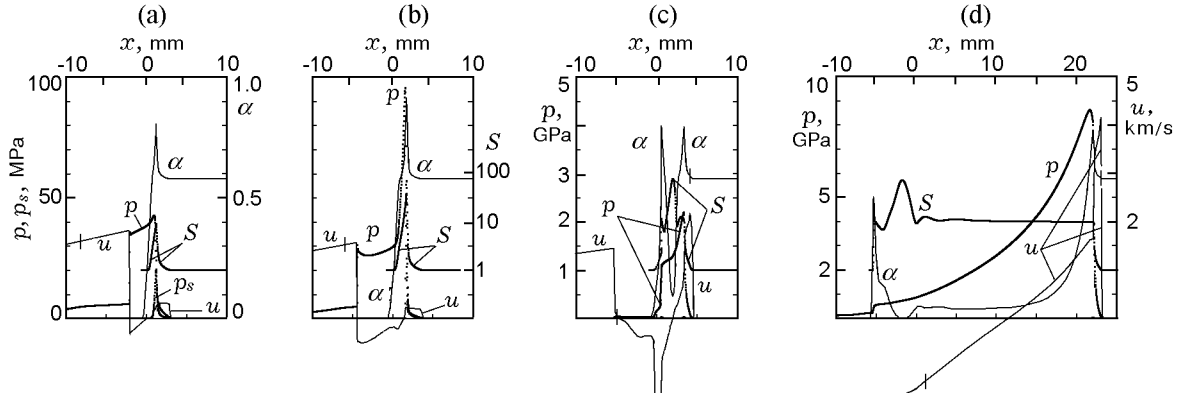


**Fig. 7.** Calculated profiles of flow parameters with allowance for the fragmentation effect at  $\Delta T_s = 20$  K: the time after the arrival of the flow on the powder boundary is 2.5 (a), 4 (b), 5 (c), and 9.5  $\mu$ s (d); the pressure scale for Figs. 7a and 7b is identical.

mation available at the time when the calculations [33] were performed, did not contradict the calculated results. New data of the synchrotron experiment allow us to obtain a much more detailed assessment of the fragmentation mechanism efficiency.

The results of modeling employing correlation (6) are shown in Fig. 7. The best agreement in terms of the wave development time is obtained for  $\Delta T_s = 20$  K (9.5  $\mu$ s, i.e., coincidence within one interval of discretization of the profiles is reached). First, the wave develops similar to Fig. 5, with the difference that fragmentation slightly intensifies the reaction. Later on, however, progressive compression converts the process to a sharper mode. At  $t = 4 \mu$ s, a clearly expressed compaction peak is formed approximately at 2 mm from the free surface of the powder, where the specific surface increases approximately by a factor of 30 (the pressure does not exceed 100 MPa). Ignition at  $\Delta T_s = 20$  K occurs at the maximum compression point. Intensification of interphase interactions by the time  $t = 5 \mu$ s leads to an increase in pressure up to 2 GPa, and the explosive in the peak practically burns out within a microsecond. It is this focus that gives rise to a rapid deflagration-to-detonation transition. The pressure  $p_s$  becomes negligibly small as compared with the gas pressure; therefore, it is not shown in Figs. 7c and 7d. At  $t = 9.5 \mu$ s, the wave passes almost over the entire charge, reaching parameters close to those of the ideal detonation regime. In this regime, the coefficient  $S$  on the wave front is close to 10, i.e., the specific surface (and the reaction rate) increase by an order of magnitude owing to fragmentation. Though the HE almost burned out in the compaction peak, the vicinity of this place retains the memory about the strong compression: the peak value of  $S$  (reflecting the degree of particle fragmentation) is of the order of 100.

The correlations used [in particular, correlation (6)] can differ from the reality at high degrees of compression. The formation of a compaction peak for an easily compressible powder, however, is inevitable. Intense fragmentation in the peak and ignition at the apex at a suitable value of  $\Delta T_s$  lead to rapid development of detonation. Strictly speaking, the wave evolution after the compaction catastrophe is beyond the framework of this model. When pressures of the order of 1 GPa are reached, the reaction mechanism should change. Indeed, at the late stage of the calculation, the reaction zone occupies approximately 5 mm, i.e., much more than it should be according to the known measurements. A shock wave is formed in the real process instead of a smooth pressure front observed in Figs. 7c and 7d, and the mechanism of hot spots is actuated. Therefore, the calculation after the compaction point is merely an illustration. At the same time, it provides an estimate from below: rapid development of detonation due to fragmentation is possible even in the case of slow kinetics of surface combustion. As the wave is accelerated rather rapidly, the allowance for the faster reaction at hot spots should not lead to noticeable changes in the total time of the process.

The calculations with other ignition temperatures demonstrate that the variants shown in Fig. 7 at  $\Delta T_s = 20$  K is the fastest one. At lower values of  $\Delta T_s$ , the combustion starts earlier. The released gas reduces the medium compressibility, which leads to smoothing of the compaction peak and to less intense development of the process. The maximum compression is reached noticeably later (for instance, at  $t = 6 \mu$ s for  $\Delta T_s = 10$  K and at  $t = 9 \mu$ s for  $\Delta T_s = 5$  K), and the wave velocity at this stage is approximately half the experimental velocity. At greater values of  $\Delta T_s = 30$ –40 K, a sharp peak arises, but the combustion occurs on its rear front,

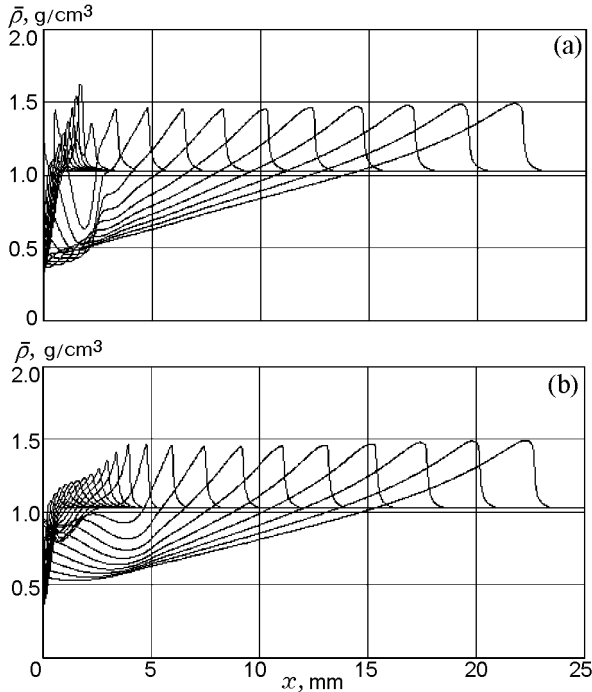


**Fig. 8.** Calculated density profiles: (a) only the fragmentation effect is taken into account (variant shown in Fig. 7), the time of the process is  $9.5 \mu\text{s}$ ; (b) other data being identical, both fragmentation and ablation with the coefficient  $k = 1$  are taken into account, the calculation time is  $11 \mu\text{s}$ ; the time step between the profiles is  $0.5 \mu\text{s}$ .

which leads to formation of an impermeable plug with extremely slow subsequent evolution.

Though the fragmentation effect provides integral agreement in terms of the detonation development time, the initial wave dynamics does not agree with the experiment. This is seen from a comparison of the experimental density profiles (see Fig. 4a) with the calculated curves (Fig. 8a). The most important feature of the model (compaction peak) is not observed in the experiment, and the density increases monotonically. Moreover, the initial stage of the process is delayed in the simulation, which is manifested as a denser network of the calculated profiles as compared with Fig. 4a. The reason for this behavior is significant inertia of the solid phase, which should be entrained by the gas flow to form the peak. One can conclude that fragmentation should be taken into account, but this factor alone is insufficient for an adequate description of experimental data.

Let us now consider the possibility of taking into account the ablation and fragmentation phenomena simultaneously. The joint effect of these mechanisms can appear as follows. Fast filtration of the gas produces

shear instability on some part of the particle surface, leading to the ablative combustion mode, whereas the remaining part of the surface experiences the action of a slower flow, leading to ignition of this part of the surface and its combustion in a slower layer-by-layer mode. Explicit consideration of these portions of the surface would be superfluous, given the current modeling level. Therefore, the kinetic coefficients of both combustion mechanisms are further understood as renormed ones (i.e., normalized to the entire specific surface of the particles).

The simulation shows that the joint action of ablation and fragmentation makes it possible to reach reasonable agreement with the experiment. Owing to intense gas release, ablation provides faster propagation of the wave at the initial stage of the process. The medium compressibility and the pressure gradient decrease; as a result, the initial compaction peak becomes less sharp or is suppressed altogether. Moderate compression of the porous bed occurs, accompanied by an increase in the specific surface. As the wave moves further, the influence of this factor is enhanced, and the role of ablation decreases.

At small values of the ablative combustion coefficient  $k$ , the results are close to the case illustrated in Figs. 7 and 8a (with the compaction peak). At high values of  $k$ , the peak is absent, but the wave develops too slowly. Reasonable agreement is reached at  $k = 1$ . The maximum density increases monotonically, as in the experiment, with an acceptable time of evolution to essentially normal detonation (with the wave velocity of  $5.1 \text{ km/s}$ ). The calculated results are shown in Fig. 8b.

Note that the ablative mechanism itself (without fragmentation) does not lead to detonation development for the charge of this size. The wave propagates with a velocity around  $0.6 \text{ km/s}$  during the first  $30 \mu\text{s}$  and is accelerated only later on. As is seen from Eq. (7), the reaction by this mechanism is sufficiently intense in places with noticeably different velocities of the phases. Because of a high flow resistance of the porous medium, the filtration velocity rapidly decreases with time. The pressure gradient necessary to support filtration decreases, and combustion becomes slower. For the same reasons, after the formation of the compression wave front, the filtration zone in the vicinity of this front is rather small. As the reaction rate (7) is proportional to  $(\rho|u - v|)^{2/3}$ , it increases slower with wave development than the standard velocity (which is proportional to pressure or  $\rho(u - v)^2$ ). Therefore, wave acceleration owing to the pure ablative mechanism is ineffective. The contribution of the standard combustion mechanism without fragmentation is not sufficient either.

## CONCLUSIONS

A new experimental approach combined with results of gas-dynamic calculations allowed us to estimate the role of various mechanisms of phase interaction in the process of rapid initiation of an HE powder by a high-enthalpy gas flow. The experimentally observed detonation development determines the requirements to the HE burning kinetics. The traditional kinetics is too slow and does not ensure initiation.

An acceptable description of the experiment was obtained by taking into account two processes intensifying the reaction simultaneously: fragmentation of particles and ablation (fast combustion provoked by shear instability of the evaporating particle surface). Each of these mechanisms separately does not provide good agreement with experimental data.

At the same time, the results obtained should be considered only as qualitative estimates. In particular, the key initial stage of the process needs a more detailed consideration. The calculated wave velocity is noticeably smaller than the experimental value during the first microseconds, and the predicted growth of density is slower. Though the ablative mechanism improves the model, one cannot argue that it solves the problem of the initial stage. For instance, a formal increase in the standard burning rate  $u_n$  by an order of magnitude could be expected to yield a similar result. Nevertheless, we can argue that it is necessary to take into account some intensification mechanism accelerating the reaction in the non-compacted material.

In particular, two processes that can accelerate the reaction at the initial stage are worth noting. The first process is combustion of the surface layer in the form of repeated flashes, which was mentioned in discussing the ignition conditions. At high heat fluxes, a rather thin HE layer is rapidly heated and ignited. The characteristic rate of regression exceeds the steady rate of regression approximately by a factor equal to the root of the ratio of the time of heating of the steady burning layer to the small time of the flash. The gases moving away from the surface decrease the heat flux, which reduces the burning rate, possibly, until complete quenching of the flame. If the flow effectively supports HE heating, however, such flashes would be periodically repeated, and the average burning rate can exceed the steady burning rate by an order of magnitude. The second process that may be important is fragmentation of particles owing to nonuniformities of aerodynamic loads on the particle surface induced by gas filtration. In contrast to fragmentation due to compaction (i.e., interaction of particles) considered above, aerodynamic fragmentation is possible without powder compaction

and can start simultaneously with gas filtration. This mechanism is responsible for destruction of meteorites in the Earth atmosphere and particles accelerated by the gas flow (see, e.g., [34]).

An unusual feature of our study, not typical for explosive processes, should be noted: we compared two-dimensional experimental data with less detailed one-dimensional calculations. The available experimental information will be used more effectively when the model dimension is increased. Moreover, it seems of interest to compare not only the density fields (density is a rather conservative variable), but also other flow fields. In the one-phase case, the problem of reconstruction of the pressure and velocity fields was solved in [16].

This work was supported by the Russian Foundation for Basic Research (Grant Nos. 09-03-00127 and 12-03-00077) and by the Scientific Program No. 2 of the Presidium of the Russian Academy of Sciences (Project No. 7).

## REFERENCES

1. J. N. Johnson, P. K. Tang, and C. A. Forest, "Shock-Wave Initiation of Heterogeneous Reactive Solids," *J. Appl. Phys.* **57** (9), 4323–4334 (1985).
2. C. M. Tarver, P. A. Urtiew, and J. W. Forbes, "Experimental and Theoretical Progress of All-Arrhenius Model of Solid Explosives Shock Initiation," *Khim. Fiz.* **20** (3), 38–42 (2001).
3. V. S. Solov'ev, "Some Specific Features of Shock-Wave Initiation of Explosives," *Fiz. Goreniya Vzryva* **36** (6), 65–76 (2000) [*Combust., Expl., Shock Waves* **36** (6), 734–744 (2000)].
4. A. F. Belyaev, V. K. Bobolev, A. I. Korotkov, et al., *Deflagration-to-Detonation Transition in Condensed Systems* (Nauka, Moscow, 1973) [in Russian].
5. A. A. Sulimov and B. S. Ermolaev, "Deflagration-to-Detonation Transition in Porous HEs," in *Detonation and Shock Waves, Proc. 8th All-Union Symposium on Combustion and Explosion* (Inst. Chemical Physics, Acad. of Sci. of the USSR, Chernogolovka, 1986), pp. 134–139.
6. R. R. Bernecker, "The Deflagration-to-Detonation Transition Process for High-Energy Propellants—A Review," *AIAA J.* **24** (1), 82–91 (1986).
7. J. M. McAfee, "The Deflagration-to-Detonation Transition," in *Non-Shock Initiation of Explosives, Shock Wave Science and Technology Reference Library*, Ed. by B. W. Asay (Springer, Berlin, Heidelberg, 2010), Vol. 5, Ch. 8, pp. 483–535.
8. J. E. Kennedy, "Impact and Shear Ignition by Non-shock Mechanisms," in *Non-Shock Initiation of Explosives, Shock Wave Science and Technology Reference Li-*

- brary, Ed. by B. W. Asay (Springer, Berlin–Heidelberg, 2010), Vol. 5, Chapter 10, pp. 555–581.
9. A. F. Belyaev, M. A. Sadovskii, and I. I. Tamm, “Application of the Similarity Law in Explosions to the Detonation Propagation Phenomenon,” *Prikl. Mekh. Tekh. Fiz.*, No. 1, 3–17 (1960).
  10. V. V. Andreev and L. A. Luk’yanchikov, “Low-Speed Detonation Mechanism in PETN Powder with Spark Ignition,” *Fiz. Goreniya Vzryva* **10** (6), 912–919 (1974) [*Combust., Expl., Shock Waves* **10** (6), 818–823 (1974)].
  11. V. V. Andreev, L. A. Luk’yanchikov, V. V. Mitrofanov, and V. S. Teslenko, “Excitation of Detonation of Powdered HEs by an Explosion of Gas Mixtures,” *Fiz. Goreniya Vzryva* **16** (5), 153–155 (1980).
  12. V. V. Grigor’ev, L. A. Luk’yanchikov, E. R. Prueel, and A. A. Vasil’ev, “Initiation of a Porous Explosive by Overdriven Gas Detonation Products,” *Fiz. Goreniya Vzryva* **37** (5), 90–97 (2001) [*Combust., Expl., Shock Waves* **37** (5), 572–579 (2001)].
  13. V. M. Aulchenko, O. V. Evdokov, I. L. Zhogin, et al., “Detector Based on a Beam of Synchrotron Radiation for Studying Explosive Processes,” *Prib. Tekh. Eksp.*, No. 3, 20–35 (2010).
  14. V. M. Aulchenko, S. E. Baru, O. V. Evdokov, et al., “Fast High Resolution Gaseous Detectors for Diffraction Experiments and Imaging at Synchrotron Radiation Beam,” *Nucl. Instrum. Methods Phys. Res. A*, **623**, 600–602 (2010).
  15. L. A. Luk’yanchikov, E. R. Prueel, A. O. Kashkarov, and K. A. Ten, “Ablation Combustion of Secondary Powder Explosives,” *Prikl. Mekh. Tekh. Fiz.* **51** (4), 5–16 (2010) [*Appl. Mech. Tech. Phys.* **51** (4), 453–462 (2010)].
  16. V. M. Titov, E. R. Prueel, K. A. Ten, et al., “Experience of Using Synchrotron Radiation for Studying Detonation Processes,” *Fiz. Goreniya Vzryva* **47** (6), 3–15 (2011) [*Combust., Expl., Shock Waves* **47** (6), 615–626 (2011)].
  17. G. E. Seay and L. B. Seely, “Initiation of a Low-Density PETN Pressing by a Plane Shock Wave,” *J. Appl. Phys.* **32** (6), 1092–1097 (1961).
  18. R. I. Nigmatulin, P. B. Vainshtein, and I. Sh. Akhatov, “Transition of Powdered Explosive Convective Combustion into Detonation,” *Fiz. Goreniya Vzryva* **19** (5), 93–97 (1983) [*Combust., Expl., Shock Waves* **19** (5), 618–621 (1983)].
  19. V. F. Kuropatenko, “Equation of State of Detonation Products of Compact Explosives,” *Fiz. Goreniya Vzryva* **25** (6), 112–117 (1989) [*Combust., Expl., Shock Waves* **25** (6), 762–767 (1989)].
  20. J. F. Baytos, B. G. Craig, A. W. Campbell, et al., *LASL Explosive Property Data* (Univ. of California Press, Berkeley, 1980).
  21. J. A. Saenz and D. S. Stewart, “Modeling Deflagration-to-Detonation Transition in Granular Explosive Pentaerythritol Tetranitrate,” *J. Appl. Phys.* **104** (4), 043519-1–043519-14 (2008).
  22. S. Ergun, “Fluid Flow through Packed Columns,” *Chem. Eng. Progr.* **48** (2), 89–94 (1952).
  23. D. P. Jones and H. Krier, “Gas Flow Resistance Measurements through Packed Beds at High Reynolds Numbers,” *Trans. ASME, J. Fluid Eng.* **105**, 168–173 (1983).
  24. W. H. Denton, “The Heat Transfer and Flow Resistance for Fluid Flow through Randomly Packed Spheres,” in *General Discussion on Heat Transfer* (Inst. of Mech. Eng. and ASME, London, 1951), pp. 370–373.
  25. I. K. Kikoin, *Tables of Physical Quantities: Reference Book* (Atomizdat, Moscow, 1976) [in Russian].
  26. B. S. Ermolaev, B. V. Novozhilov, V. S. Posvyanskii, and A. A. Sulimov, “Results of Numerical Modeling of the Convective Burning of Particulate Explosive Systems in the Presence of Increasing Pressure,” *Fiz. Goreniya Vzryva* **21** (5), 3–12 (1985) [*Combust., Expl., Shock Waves* **21** (5), 505–513 (1985)].
  27. E. A. Averson, V. V. Barzykin, and A. G. Merzhanov, “Approximate Method of Solving Problems of the Thermal Theory of Ignition,” *Dokl. Akad. Nauk SSSR* **178** (1), 131–134 (1968).
  28. A. G. Merzhanov and A. E. Averson, “The Present State of the Thermal Ignition Theory: An Invited Review,” *Combust. Flame* **16** (1), 89–124 (1971).
  29. R. N. Rogers, “Thermochemistry of Explosives,” *Thermochim. Acta* **11** (2), 131–139 (1975).
  30. S. G. Andreev, A. S. Babkin, F. A. Baum, et al., *Physics of Explosion* (Fizmatlit, Moscow, 2004) [in Russian].
  31. K. K. Andreev, *Thermal Decomposition and Combustion of High Explosives* (Nauka, Moscow, 1966) [in Russian].
  32. V. V. Andreev, A. P. Ershov, and L. A. Luk’yanchikov, “Two-Phase Low-Speed Detonation of a Porous Explosive,” *Fiz. Goreniya Vzryva* **20** (3), 89–93 (1984) [*Combust., Expl., Shock Waves* **20** (3), 330–334 (1984)].
  33. A. P. Ershov, “Modeling of the Deflagration to Detonation Transition in Porous PETN,” in *Proc. 11th Symp. (Int.) on Detonation* (Snowmass Village, 1998), pp. 686–692.
  34. V. M. Titov, Yu. I. Fadeenko, and N. S. Titova, “Acceleration of Solids by a Cumulative Explosion,” *Dokl. Akad. Nauk SSSR* **180** (5), 1051–1052 (1968).